Inorganic Chemistry

Article

pubs.acs.org/IC

Host-Sensitized Luminescence Properties in $CaNb_2O_6$:Ln^{3+} (Ln^{3+} = Eu^{3+}/Tb^{3+}/Dy^{3+}/Sm^{3+}) Phosphors with Abundant Colors

Kai Li,[†,§] Xiaoming Liu,[‡] Yang Zhang,[†,§] Xuejiao Li,[†] Hongzhou Lian,*[,†] and Jun Lin*[,†]

[†]State Key Laboratory of Rare Earth Resource Utilization, Changchun Institute of Applied Chemistry, Chinese Academy of Sciences, Changchun 130022, P. R. China

[‡]School of Environment and Chemical Engineering, Nanchang Hangkong University, Nanchang 330063, P. R. China

[§]University of Chinese Academy of Sciences, Beijing 100049, P. R. China

ABSTRACT: A series of Ln^{3+} (Ln^{3+} = Eu^{3+}/Tb^{3+}/Dy^{3+}/Sm^{3+}) ion doped $CaNb_2O_6$ (CNO) phosphors have been prepared via the conventional high-temperature solid-state reaction route. The X-ray diffraction (XRD) and structure refinement, diffuse reflection, photoluminescence (PL), and fluorescent decay curves were used to characterize the as-prepared samples. Under UV radiation, the CNO host present a broad emission band from about 355 to 605 nm centered around 460 nm originating from the NbO_6 octahedral groups, which has spectral overlaps with the excitation of f−f transitions of Eu^{3+}/Tb^{3+}/Dy^{3+}/Sm^{3+} in CNO:Eu^{3+}/Tb^{3+}/Dy^{3+}/Sm^{3+} samples. They show both host emission and respective emission lines derived from the characteristic f−f transitions of activators, which present different emission colors owing to the energy transfer from the NbO_6 group in the host to Eu^{3+}/Tb^{3+}/Dy^{3+}/Sm^{3+} with increasing activator concentrations. The decreases of decay lifetimes of host emissions in CNO:Eu^{3+}/Tb^{3+}/Dy^{3+}/Sm^{3+} demonstrate the energy transfer from the hosts to Eu^{3+}/Tb^{3+}/Dy^{3+}/Sm^{3+}. The energy transfer mechanisms in CNO:Eu^{3+}/Tb^{3+}/Dy^{3+} phosphors have been determined to be a resonant type via dipole−dipole mechanisms. For CNO:Sm^{3+}, the metal−metal charge transfer transition (MMCT) might contribute to the different variations of decay lifetimes and emission intensity from CNO:Eu^{3+}/Tb^{3+}/Dy^{3+} samples. The best quantum efficiency is 71.2% for CNO:0.01/0.02Dy^{3+}. The PL properties of as-prepared materials indicate the promising application in UV-pumped white-emitting lighting diodes field.

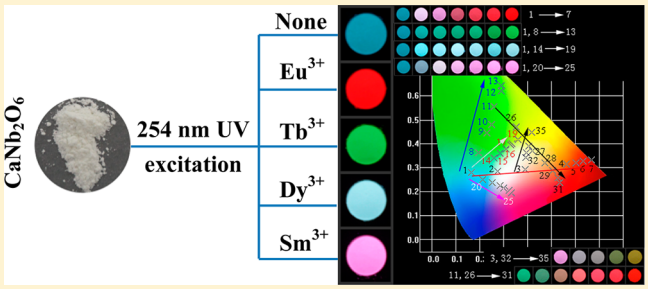

1. INTRODUCTION

Recently, rare earth ions-doped oxide luminescent materials involving good thermal and chemical stability have attracted much attention since they can be extensively used in display devices (e.g., cathode ray tubes, field emission displays, and vacuum fluorescent displays), lighting apparatus (e.g., fluorescent tubes and white light-emitting diodes), solid-state laser, biological labeling, medical devices, X-ray, ionizing radiation, and so on.[1−11] Among them, white light-emitting diodes (WLEDs) have been considered to be the next generation illumination source instead of current conventional incandescent and fluorescent lamps because of their superior merits such as energy saving, high energy efficiency, no environmental contamination, and long operation time. Compared with conventional methods (InGaN chip + $Y_3Al_5O_{12}$:Ce^{3+} phosphor), coating UV LEDs chips with tricolor (blue, green, red) phosphors is being investigated to obtain WLEDs because low correlated color temperature (CCT) and high rending index (CRI) can be realized via this method.[12−16] With the development of $Ga_xAl_{1-x}N$ LED chips, its emitting wavelength has been extended to 330 nm by adjusting the value of x.[17] Therefore, we can expect that the shorter emitting wavelength would be realized in near future based on the demand of more efficient excitation by higher energy for rare earth ions.

Generally, it is vital to select appropriate compounds as the hosts for rare earth ions to accommodate as the luminescent activators; however, the hosts also can emit visible light owing to their proper band gap in some compounds.[18−22] These activators often have excitation energy levels that can be excited by direct excitation or indirect energy transfer from the host, which can emit abundant colors based on their 4f−4f or 5d−4f transitions. As an importantly used red emitting activator, the Eu^{3+} ion shows its characteristic emissions originating from the transitions of $^5D_{0,1,2}$−^7F_J (J = 4, ..., 0). Also, the Tb^{3+}, Dy^{3+}, and Sm^{3+} ions-doped phosphors are often applied as green, white, and light red materials on the basis of their characteristic transitions of $^5D_4$−^7F_J (J = 3, 4, 5, and 6), $^4F_{9/2}$-$^6H_{15/2}$ (blue) and $^4F_{9/2}$−$^6H_{13/2}$ (yellow), and $^4G_{5/2}$-^6H_J (J = 5/2,7/2,9/2 and 11/2), respectively. The f−f transitions Ln^{3+} ions generally have low excitation efficiencies because of their forbidden parity selection rules. Thus, utilizing the host sensitization via energy transfer from the excited host to Ln^{3+} ions is an effective way to overcome the above drawback in many phosphors such as $Ca_{0.5}Sr_{0.5}MoO_4$:Dy^{3+},[23] $GdPO_4$:Dy^{3+},[24] $LiInW_2O_8$:Eu^{3+},[25] and Gd_2MoO_6:Sm^{3+}.[26]

Received: October 11, 2014
Published: December 11, 2014

   dx.doi.org/10.1021/ic502493c | Inorg. Chem. 2015, 54, 323−333

Niobates have attracted a great deal of attention in several devices due to their commendable electro-optical, photoelastic, piezo-electric, and nonlinear properties together with good mechanical and chemical stability and a wide transparency range.[27,28] The luminescence properties of rare earth ions-doped phosphors such as $YNbO_4:Eu^{3+}$, $GdNbO_4:Tm^{3+}$, Dy^{3+}, and $La_3NbO_7:Eu^{3+}$ have been investigated in detail,[27,29,30] which are related to the host sensitization via energy transfer from host to activators based on energy matching of host photoluminescence (PL) emission and activators excitation spectra. $CaNb_2O_6$, a subcomponent of the complex perovskite family $A(B'_{1/3}B''_{2/3})O_3$, crystallizing with orthorhombic columbite structure in the space group of *Pbcn*(60), has been investigated as a blue luminescence material, a good dielectric material for microwave dielectric applications, a catalyst for photocatalytic splitting of water, a strong source of coherent light which can be useful in applications of holography, as well as laser host material.[31−35] In 2007, Boutinaud et al. have investigated the dependence of PL properties of Tb^{3+}-doped $CaNb_2O_6$ on temperature.[36] In 2011, Huang et al. have shown the PL of $CaNb_2O_6:Eu^{3+}$ under 393 nm excitation.[37] Recently, Wang et al. report ed the synthesis of $CaNb_2O_6:Sm^{3+}$ thin films by pulsed laser deposition.[38] However, the investigations on PL and energy transfer properties of Eu^{3+}-, Tb^{3+}-, Dy^{3+}-, and Sm^{3+}-doped $CaNb_2O_6$ (CNO) phosphors under excitation of host absorption band have been rarely performed. Therefore, we present the PL properties of a series of phosphors excited by host absorption band with the composition of CNO:Eu^{3+}/Tb^{3+}/Dy^{3+}/Sm^{3+} in detail. In addition, the XRD profiles refinements, discussions of crystallographic sites occupation and energy transfer (from the host to the activators) mechanisms have been conducted. It suggests that they would have good potential in the solid-state lighting field.

2. EXPERIMENTAL SECTION

2.1. Materials and Preparation. A series of phosphors with the chemical composition of $Ca_{(1-x/y/z/l)}Nb_2O_6:xEu^{3+}/yTb^{3+}/zDy^{3+}/lSm^{3+}$ (x = 0−0.36, y = 0−0.16, z = 0−0.10, l = 0−0.12), where Ca atoms occupations were considered to be substituted by rare earth atoms, were synthesized via the conventional high-temperature solid-state reaction route. Typically, stoichiometric amounts of raw materials without further purification, namely, $CaCO_3$ (A.R.), Nb_2O_5 (A.R.), Eu_2O_3 (99.99%), Tb_4O_7 (99.99%), Dy_2O_3 (99.99%), Sm_2O_3 (99.99%), were employed and thoroughly combined in an agate mortar for about 15 min by adding an appropriate amount of ethanol followed by drying for about 20 min. Then, the powder mixtures were loaded into the crucibles and transferred to the box furnace to calcine at 1250 °C for 7 h in air condition to produce the final samples after being reground for 1 min.

2.2. Characterization. The X-ray diffraction (XRD) patterns were obtained on a D8 Focus diffractometer at a scanning rate of 10° min^{-1} in the 2θ range from 10° to 110° with graphite-monochromatized Cu Kα radiation (λ = 0.15405 nm). The General Structure Analysis System (GSAS) program was used to conduct the structure refinements. Diffuse reflectance spectral measurement was carried on with a Hitachi U-4100-Vis/NIR spectrophotometer. The PL spectra were recorded by a Hitachi F-7000 spectrophotometer with a different excitation source (a 150 W xenon lamp and electron beam, respectively). The fluorescent decay curves were measured by a Lecroy Wave Runner 6100 Digital osilloscope (1 GHz) using a tunable laser (pulse width = 4 ns, gate = 50 ns) as the excitation source (Contimuum Sunlite OPO). PL quantum yields (QYs) were obtained directly by the absolute PL quantum yield (internal quantum efficiency) measurement system (C9920-02, Hamamatsu Photonics K. K., Japan), involving an excitation light source of a Xe lamp, a monochromator, an integrating sphere capable of nitrogen gas flow, together with a CCD spectrometer for detecting the whole spectral range, simultaneously. All the measurements were conducted at room temperature (RT).

3. RESULTS AND DISCUSSION

3.1. Phase Identification and Structure. The composition, phase purity, and crystal structure of as-prepared representative samples CNO host, CNO:0.04Eu^{3+}, CNO:0.04Tb^{3+}, CNO:0.04Dy^{3+}, and CNO:0.04Sm^{3+} were first identified by XRD patterns, which are clearly shown in Figure 1. All the diffraction peaks match well with that of the

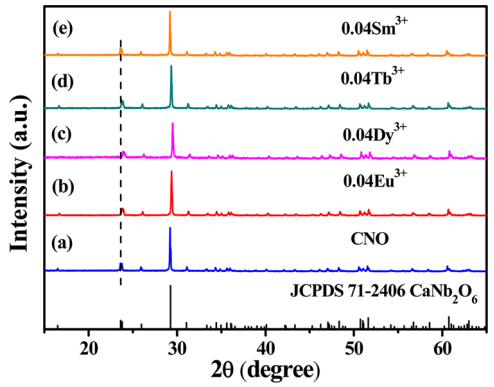

Figure 1. XRD patterns of representative CNO host (a), CNO:0.04Eu^{3+} (b), CNO:0.04Dy^{3+} (c), CNO:0.04Tb^{3+} (d), CNO:0.04Sm^{3+} (e) samples and the reference for standard card of $CaNb_2O_6$ (JCPDS no. 71-2406).

orthorhombic columbite $CaNb_2O_6$ phase according to the standard reference of JCPDS card no. 71-2406, and no traces of impurity phases are observed, indicating little change of this crystal structure when introducing such Eu^{3+}, Tb^{3+}, Dy^{3+}, and Sm^{3+} ions into the host. As shown in Figure 2a, $CaNb_2O_6$ crystallizes in an orthorhombic columbite structure in the space group of *Pbcn*(60) with the cell parameters of a = 14.926(4) Å, b = 5.752(4) Å, c = 5.204(4) Å, V = 446.79 $Å^3$, Z = 4,[39] which possesses a low-symmetry crystal structure, and the Ca and Nb cations are both at the center of octahedrons surrounded by six oxygen atoms. The CaO_6 and NbO_6 octahedron form independent zigzag chains by sharing edges, and the chains are connected by sharing corners in the order of CaO_6 chain-NbO_6 chain-NbO_6 chain.[40] There is only one kind of Ca cationic site with Wyckoff position 4c for activators to accommodate based on their similar ionic radius of Ca^{2+} [r = 1.00 Å for coordination number (CN) = 6] and Sm^{3+} (r = 0.96 Å for CN = 6), Eu^{3+} (r = 0.95 Å for CN = 6), and Tb^{3+} (r = 0.92 Å for CN = 6), Dy^{3+} (r = 0.91 Å for CN = 6). Also, the slight shift of the XRD patterns of CNO: Eu^{3+}/Tb^{3+}/Dy^{3+}/Sm^{3+} relevant to the CNO host can be observed and attributed to the different radii between Ca^{2+} and rare earth ions. In order to further recognize the effect to crystal structure of doping rare earth ions, the Rietveld refinements of powder XRD profiles of representative CNO host, CNO:0.04Eu^{3+}, CNO:0.04Tb^{3+}, CNO:0.04Dy^{3+} ,and CNO:0.04Sm^{3+} were conducted by the general structure analysis system (GSAS) method, and the refinement results are presented in detail in Table 1. The original structure model of previously reported crystallographic data of $CaNb_2O_6$ (ICSD #15208) was employed to refine the above samples. The experimental, calculated, and difference XRD profiles and Bragg positions for the Rietveld refinements

dx.doi.org/10.1021/ic502493c | Inorg. Chem. 2015, 54, 323−333

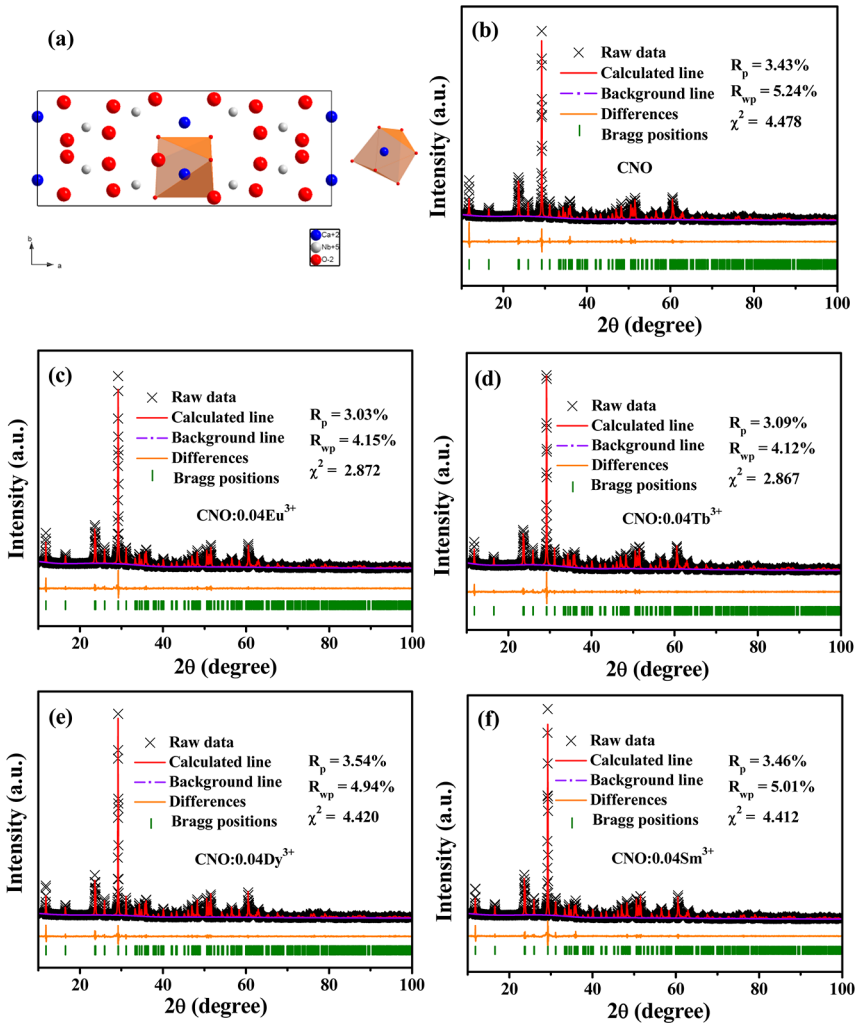

Figure 2. (a) The crystal structure of $CaNb_2O_6$, and the Rietveld refinements of powder XRD profiles of representative CNO host (b), CNO:0.04Eu^{3+} (c), CNO:0.04Tb^{3+} (d), CNO:0.04Dy^{3+} (e), and CNO:0.04Sm^{3+} (f) samples.

Table 1. Final Parameters for Crystallography and Refinement Results for CNO Host and CNO:Ln^{3+} (Ln^{3+} = Eu^{3+}/Tb^{3+}/Dy^{3+}/Sm^{3+}) Samples

formula	$CaNb_2O_6$	$Ca_{0.96}Eu_{0.04}Nb_2O_6$	$Ca_{0.96}Tb_{0.04}Nb_2O_6$	$Ca_{0.96}Dy_{0.04}Nb_2O_6$	$Ca_{0.96}Sm_{0.04}Nb_2O_6$
crystal system	orthorhombic	orthorhombic	orthorhombic	orthorhombic	orthorhombic
space group	P_{bcn}	P_{bcn}	P_{bcn}	P_{bcn}	P_{bcn}
a/Å	14.9806(2)	14.9825(3)	14.9788(2)	14.9748(2)	14.9805(2)
b/Å	5.7494(1)	5.7464(1)	5.7462(1)	5.7445(1)	5.7460(1)
c/Å	5.2243(1)	5.2252(1)	5.2242(1)	5.2221(1)	5.2244(1)
V/Å^3	449.97(1)	449.86(2)	449.65(1)	449.29(1)	449.70(1)
Z	4	4	4	4	4
radiation type	Cu−K_α	Cu−K_α	Cu−K_α	Cu−K_α	Cu−K_α
wavelength/Å	1.5418	1.5418	1.5418	1.5418	1.5418
profile range/°	10−110	10−110	10−110	10−110	10−110
R_p/%	3.43	3.03	3.09	3.54	3.46
R_{wp}/%	5.24	4.15	4.12	4.94	5.01
χ^2	4.478	2.872	2.867	4.420	4.412

of CNO host, CNO:0.04Eu^{3+}, CNO:0.04Tb^{3+}, CNO:0.04Dy^{3+}, and CNO:0.04Sm^{3+} at room temperature are shown in Figure 2b−f, respectively, further indicating that introducing rare earth ions into this host has little influence to the crystal structure of $CaNb_2O_6$.

3.2. Photoluminescence Properties. As depicted in Figure 3, the reflectance spectra of CNO, CNO:0.04Eu^{3+}, CNO:0.04Tb^{3+}, CNO:0.04Dy^{3+}, and CNO:0.04Sm^{3+} phosphors show similar profiles, which illustrates that the absorptions of dopant samples derive from the host. The reflectance spectra present strong energy absorption bands in the region of 220−350 nm, corresponding to the charge transfer band (CTB) from O ligands to central Nb atoms in the NbO_6 octahedral groups. In order to assess the absorption edge

dx.doi.org/10.1021/ic502493c | Inorg. Chem. 2015, 54, 323−333

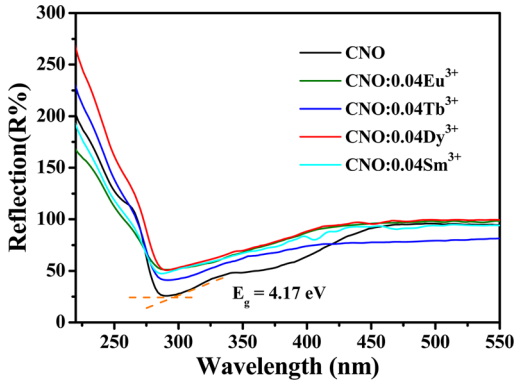

Figure 3. Diffuse reflection spectra of CNO host, CNO:0.04Eu^{3+}/0.04Tb^{3+}/0.04Dy^{3+}/0.04Sm^{3+}.

from the reflectance spectra, the Kubelka–Munk absorption coefficient (K/S) relationship was availed as follows:[41−43]

$$(1 - R)^2/2R = K/S \quad (1)$$

where K refers to the absorption coefficient, R represents the reflectivity, and S is the scattering coefficient. From the reflectance spectrum of host, a roughly evaluated optical band gap is 4.17 eV, which coincides with the PL excitation spectrum of the host in Figure 4a. Figure 4a clearly illustrates a broad

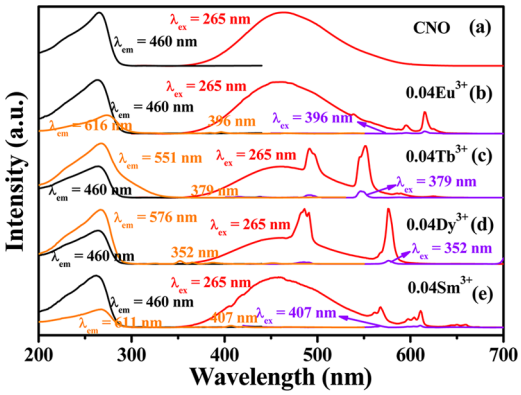

Figure 4. PL emission and excitation spectra of CNO host (a), CNO:0.04Eu^{3+}/0.04Tb^{3+}/0.04Dy^{3+}/0.04Sm^{3+} (b–e).

emission band centered at 460 nm with the extent from 355 to 605 nm, which generally presents the cyan color upon 265 nm UV excitation for the CNO host. Monitored at 460 nm, a wide excitation band peaking at 265 nm in the range of 200–300 nm is observed. In general, a large number of free holes in the valence band (VB) and electrons in the conduction band (CB) can be respectively produced when excited by UV radiation. Then the corresponding self-trapped holes (STHs) are swiftly yielded from the transformation of as-achieved free holes. However, some unsaturated atoms and unpaired electrons are generally situated in the surface regions to generate some localized levels in the forbidden gaps. Some electrons are transited to these localized levels under expected energy excitation; thus certain polarons as captured centers will appear and interact with the STHs to generate self-trapped excitons (STEs). At last, the recombination of these excitons results in the broad emission band.[44] Monitored at 616 nm, the PL excitation spectrum of CNO:0.04Eu^{3+} displays a broad band ranging from 200 to 305 nm (Figure 4b, orange line) with the maximum at 273 nm, which is similar but a tiny difference from that of host monitored at 460 nm (Figure 4b, black line), and some weak narrow peaks (363, 384, 396, 418, 467, and 538 nm, respectively) resulting from the combined absorptions of host and Eu^{3+}-O^{2-} CT transition, as well as 4f–4f characteristic transitions of Eu^{3+} in Figure 4b, respectively. Upon the excitation of CTB transition centered at 265 nm, the emission spectrum presents both the wide host emission band and the characteristic emission lines deriving from the 4f–4f transitions of Eu^{3+} ions in CNO:0.04Eu^{3+}, namely, $^5D_{0,1}$ excited states to the ^7F_J ground states including $^5D_1 \rightarrow {}^7F_1$ (539 nm), $^5D_0 \rightarrow {}^7F_1$ (595 nm), $^5D_0 \rightarrow {}^7F_2$ (616 nm), and $^5D_0 \rightarrow {}^7F_3$ (626 nm), respectively, in which the intensity of the electric dipole transition $^5D_0 \rightarrow {}^7F_2$ around 616 nm is much stronger than that of the magnetic dipole $^5D_0 \rightarrow {}^7F_1$ around 593 nm, implying that the Eu^{3+} ions easily occupy the sites without or deviated from inversion symmetry. On account of the similar ion sizes, Eu^{3+} ions would like to substitute the Ca^{2+} in lattice sites. Similarly, when a small number of Sm^{3+} ions are doped into the host and excited into the CTB transition centered at 265 nm, the emission band contains not only host emission but also the characteristic emission lines corresponding to the main transitions of $^4G_{5/2} \rightarrow {}^6H_{J=5/2,\ 7/2,\ 9/2}$ (568, 611, and 651 nm, respectively) transitions of Sm^{3+} and the wavelength of PL excitation spectrum monitored at 611 nm with the strongest intensity produces a minute red shift compared to the host excitation spectrum detected at 460 nm owing to the combination of host absorption and Sm^{3+}-O^{2-} CT transition, as shown in Figure 4e. Figure 4c,d shows the respective PL excitation and emission spectra of CNO:0.04Tb^{3+} and CNO:0.04Dy^{3+}. In the excitation spectra monitored by the emission peaks of the Tb^{3+} $^5D_4 \rightarrow {}^7F_5$ transition at 551 nm (Figure 4c, orange line), a similar wide band with a maximum around 265 nm can be observed, whereas the excitation spectral edge is extended to about 350 nm, which would be attributed to the combination of CT from the oxygen ligands to the central niobium atom within the NbO_6 octahedral group and the 4f–5d transition of Tb^{3+} ion. As to the Dy^{3+} $^4F_{9/2} \rightarrow {}^6H_{13/2}$ transition at 576 nm (Figure 4d, orange line), a broad band similar to host excitation spectrum appears to be attributed to the CT from the oxygen ligands to the central niobium atom within the NbO_6 octahedral groups. The characteristic excitation lines profiles of Tb^{3+} or Dy^{3+} can almost not be detected for the reason that the absorption intensity of the general f–f transition within the $4f^8$ or $4f^9$ configuration corresponding to Tb^{3+} or Dy^{3+} ion is much weaker than that of the NbO_6 groups, which implies the excitation of Tb^{3+} or Dy^{3+} is primarily originated from the energy transfer from host to the activators. Upon excitation into the NbO_6 group at 265 nm, the characteristic emission lines involving 491 nm ($^5D_4 \rightarrow {}^7F_6$), 551 nm ($^5D_4 \rightarrow {}^7F_5$), 589 nm ($^5D_4 \rightarrow {}^7F_4$), and 624 nm ($^5D_4 \rightarrow {}^7F_3$) of the Tb^{3+} ion, 487 nm ($^4F_{9/2} \rightarrow {}^6H_{15/2}$) and 576 nm ($^4F_{9/2} \rightarrow {}^6H_{13/2}$) of the Dy^{3+} ion, together with the broad host emission band centered at 460 nm, can be clearly observed. Upon activators characteristic 4f–4f transitions excitation wavelengths at 396, 379, 352, and 407 nm, the unique emission bands (violet lines in Figure 4b–e) of Eu^{3+}, Tb^{3+}, Dy^{3+}, and Sm^{3+} can be detected and are much weaker than those of the CTB transition, respectively, which illustrates that a non-resonant and phonon-assisted mechanism would play an important role in the energy transfer process but is not the predominant one. Upon UV excitation, a part of the excited free electrons could be first delocalized accompanied by the

dx.doi.org/10.1021/ic502493c | Inorg. Chem. 2015, 54, 323–333

autoionization process in $Eu^{3+}/Tb^{3+}/Dy^{3+}/Sm^{3+}$ doped CNO system, after which the activators as $Eu^{3+}/Tb^{3+}/Dy^{3+}/Sm^{3+}$ could capture the exciton along with the exciton recombination process. Therefore, part of the energy could be transferred to $Eu^{3+}/Tb^{3+}/Dy^{3+}/Sm^{3+}$ ions via resonant energy transfer mechanism, such as exchange interactions or multipole interactions.[45,46] We can deduce that the energy transfers primarily take place from the NbO_6 groups of host to $Eu^{3+}/Tb^{3+}/Dy^{3+}/Sm^{3+}$ by the spectral overlaps between the emission bands of host and the characteristic excitation spectra of $Eu^{3+}/Tb^{3+}/Dy^{3+}/Sm^{3+}$ in phosphors, as illustrated in Figure 5. Figure

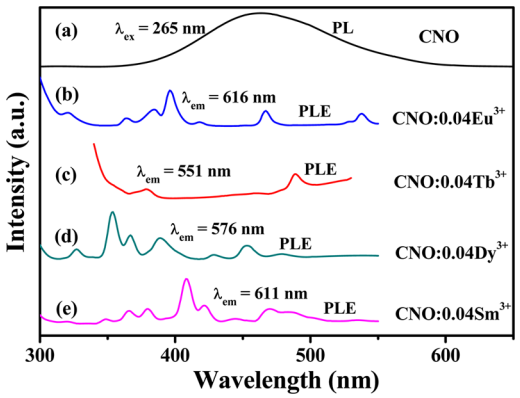

Figure 5. PL emission spectrum of CNO (a) and PL characteristic excitation spectra of activators in $CNO:0.04Eu^{3+}/0.04Tb^{3+}/0.04Dy^{3+}/0.04Sm^{3+}$ (b–e).

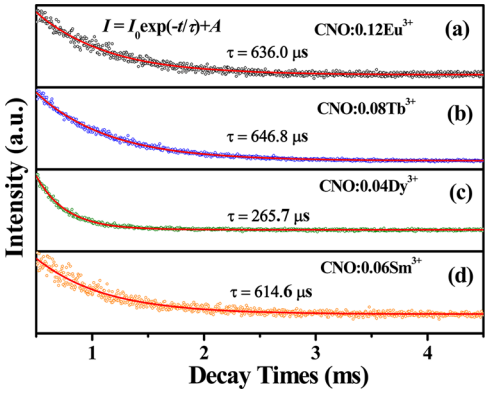

Figure 6. Decay curves of activators characteristic emissions in $CNO:0.12Eu^{3+}$ at 616 nm (a), $CNO:0.08Tb^{3+}$ at 551 nm (b), $CNO:0.04Dy^{3+}$ at 576 nm (c) and $CNO:0.06Sm^{3+}$ at 611 nm (d) excited at 265 nm.

6 presents the decay curves of activators characteristic emissions in $CNO:0.12Eu^{3+}$ (616 nm), $CNO:0.08Tb^{3+}$ (551 nm), $CNO:0.04Dy^{3+}$ (576 nm), and $CNO:0.06Sm^{3+}$ (611 nm) excited at 265 nm, which can be well fitted with a single-exponential formula as follows:[47–49]

$$I = I_0 \exp(-t/\tau) + A \quad (2)$$

where I refers to the fluorescent intensity, I_0 represents a constant, t is the time, and τ corresponds to the decay lifetime for the exponential component, A is the value for different fittings. The values of lifetime are determined to be 636.0, 646.8, 265.7, and 614.6 μs for Eu^{3+}, Tb^{3+}, Dy^{3+}, and Sm^{3+}, respectively, which are consistent with the previous results in refs 50–53 and much longer than that of the host emission below in Figure 10. These results illustrate that the characteristic emission spectra of Ln^{3+} ions can appear in this kind of host.

Figure 7a–d shows the various PL emission spectra for $CNO:xEu^{3+}/yTb^{3+}/zDy^{3+}/lSm^{3+}$ (x = 0–0.36, y = 0–0.16, z = 0–0.10, l = 0–0.12) with different concentrations of Ln^{3+} ions, respectively. We can observe the emission intensities of host decrease sharply with the increases of $Eu^{3+}/Tb^{3+}/Dy^{3+}/Sm^{3+}$ concentrations under the excitation of 265 nm UV. However, the emission intensities of $Eu^{3+}/Tb^{3+}/Dy^{3+}$ in the $CNO:xEu^{3+}/yTb^{3+}/zDy^{3+}$ systems clearly increase to the maximum at x = 0.30, y = 0.08, and z = 0.06, respectively, and subsequently descend with respectively further concentration of Ln^{3+} ions resulting from the concentration quenching effects in Figure 7a–c. Differently, the emission intensity of $CNO:lSm^{3+}$ monitored at 611 nm keeps low and changes a little with the increase of Sm^{3+} concentration in Figure 7d. This phenomenon may be ascribed to the metal–metal charge transfer transition (MMCT) of $Nb^{5+} + Sm^{3+} \rightarrow Nb^{4+} + Sm^{4+}$ because Nb^{5+} has a tendency to be reduced, whereas Sm^{3+} possesses a tendency to be oxidized to quadrivalence, forming the Nb^{4+}-Sm^{4+} CT state similar to $Ce^{3+}/Pr^{3+}/Tb^{3+}$ in YVO_4 host.[54] Therefore, the excited electrons can be readily transferred to the Nb^{4+}-Sm^{4+} CT state followed by the nonradiative relaxation to the ground state of Sm^{3+}, leading to the loss of emission energy of Sm^{3+}. Those detailed variations of host and activators emission intensities are presented in Figure 8. The energy transfer efficiencies (η_T) from the host to activators in $CNO:xEu^{3+}/yTb^{3+}/zDy^{3+}/lSm^{3+}$ systems were calculated using the equation $\eta_T = 1 - I_S/I_{S_0}$,[55–58] where η_T refers to the energy transfer efficiencies, and I_{S_0} and I_S are the luminescence intensities of the host with and without an activator ($Eu^{3+}/Tb^{3+}/Dy^{3+}/Sm^{3+}$), respectively. As depicted in Figure 9, the η_T values from host to activators in $CNO:xEu^{3+}/yTb^{3+}/zDy^{3+}/lSm^{3+}$ systems are plotted as a function of concentrations of $Eu^{3+}/Tb^{3+}/Dy^{3+}/Sm^{3+}$ ions, which show that the η_T values monotonously increase to reach maximums at 98%, 80%, 67%, and 72% under 265 nm UV radiation, respectively, indicating the energy transfer from the NbO_6 group in the host to activators becomes more and more efficient with the increasing concentration of activators ions. However, most of the energy from host absorption in $CNO:Sm^{3+}$ has been lost due to the MMCT effect.

The fluorescent decay lifetimes measurements for the host emission (λ_{ex} = 265 nm, λ_{em} = 460 nm) were conducted to further verify the occurrence energy transfer from host to activators. As illustrated in Figure 10a–d, the decay curves are clearly plotted with increasing activators concentrations. Generally, double-exponential decay behavior of the activator is frequently observed when the excitation energy is transferred from the sensitizer to activator. Therefore, all of them can be well fitted using a second-order exponential function, and their corresponding decay times can be calculated by the following equation:[59–62]

$$I = I_0 + A_1 \exp(-t/\tau_1) + A_2 \exp(-t/\tau_2) \quad (3)$$

where I and I_0 represents the luminescence intensities at time t and 0, τ_1 and τ_2 refer to two components of the luminescence lifetime, which correspond to the rapid and slow lifetimes for exponential components, respectively; A_1 and A_2 are constants;

dx.doi.org/10.1021/ic502493c | Inorg. Chem. 2015, 54, 323–333

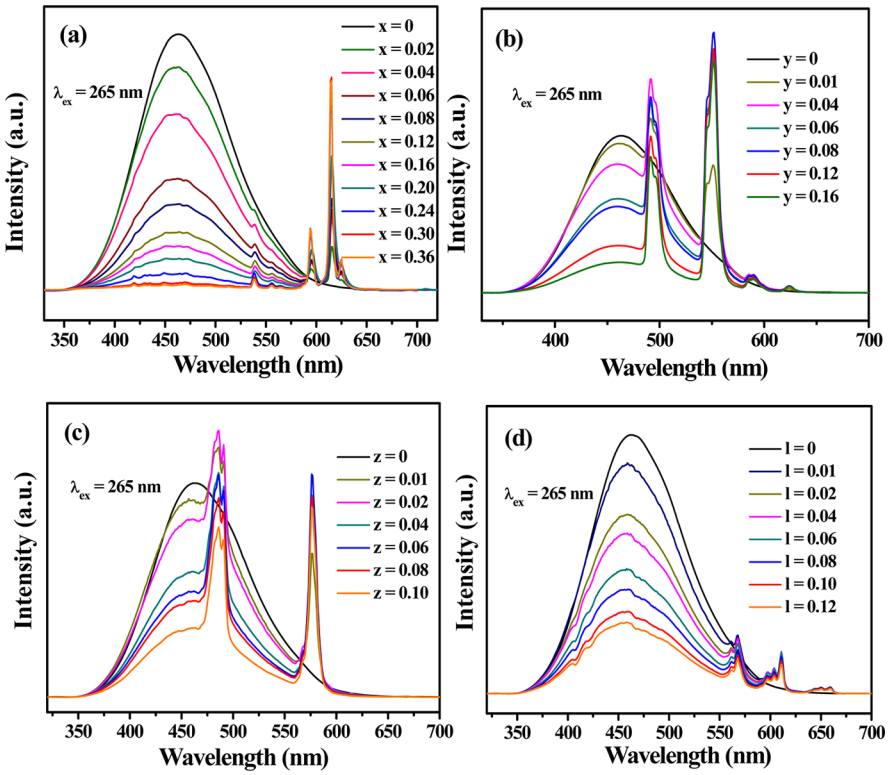

Figure 7. Dependence of PL emission spectra of CNO:xEu^{3+}/yTb^{3+}/zDy^{3+}/lSm^{3+} excited at 265 nm on their concentrations [x = 0–0.36 (a), y = 0–0.16 (b), z = 0–0.10 (c), l = 0–0.12 (d)].

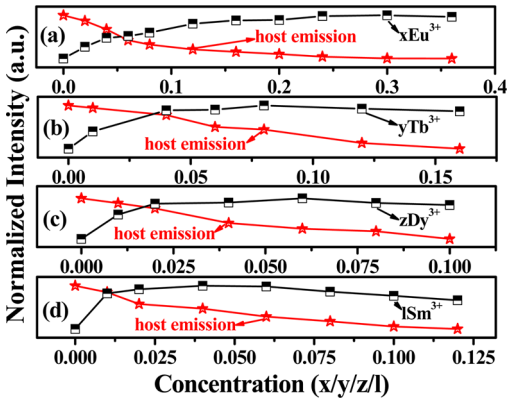

Figure 8. Variation of emission intensity of host and activators on concentrations of rare earth ions in CNO:xEu^{3+}/yTb^{3+}/zDy^{3+}/lSm^{3+} (a–d) phosphors, respectively.

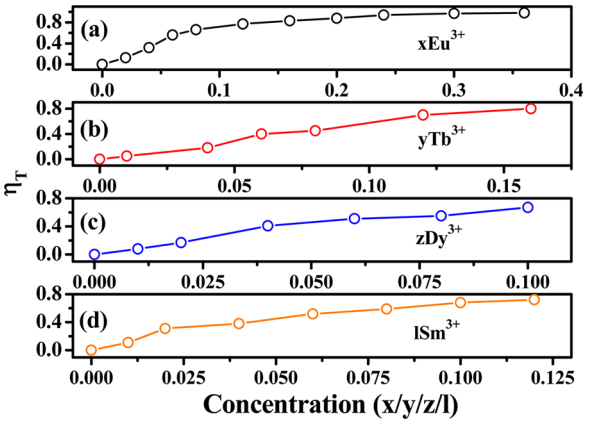

Figure 9. Energy transfer efficiencies (η_T) from host to activators in CNO:xEu^{3+} (a), CNO:yTb^{3+} (b), CNO:zDy^{3+} (c), CNO:lSm^{3+} (d).

t is the time. According to these parameters, the average decay times (τ) can be determined by the following formula:

$$\tau = (A_1\tau_1^2 + A_2\tau_2^2)/(A_1\tau_1 + A_2\tau_2) \quad (4)$$

The values of calculated decay lifetimes are summarized and displayed in Table 2. We can observe that the average decay times (τ) of host emission is 56.25 ns without any doping of Ln^{3+} ions. With the increasing concentration of dopant ions, the value of τ of host emission monotonously decreases from 56.25 to 34.18, 36.60, and 43.34 ns for CNO:Eu^{3+}, CNO:Tb^{3+}, and CNO:Dy^{3+}, respectively, which can well certify the existence of energy transfer from host to activators (Eu^{3+}/Tb^{3+}/Dy^{3+}). However, when Sm^{3+} were doped into host, the value of τ of host emission for CNO:0.02Sm^{3+} sample is smaller than that of matrix first and then becomes a various rather than monotonous decrease with further doping concentration of Sm^{3+} in Figure 10d, which implies that the combination of energy transfer from the host to Sm^{3+} ions and the MMCT effect would contribute to this phenomenon. Therefore, the energy transfer mechanism from the host to Sm^{3+} ions in CNO:Sm^{3+} samples is difficult to determine.

3.3. Energy Transfer Mechanism. In order to determine the energy transfer mechanisms from host to activators in CNO:Eu^{3+}/Tb^{3+}/Dy^{3+} samples, it is necessary to know the critical distance (R_c) between activators such as Eu^{3+}/Tb^{3+}/Dy^{3+} here. With the increasing Eu^{3+}/Tb^{3+}/Dy^{3+} contents, the energy transfer from the host to activators becomes more efficient, and the probability of energy migration between activators increases simultaneously. When the distance is small enough, the concentration quenching occurs and the energy

dx.doi.org/10.1021/ic502493c | Inorg. Chem. 2015, 54, 323–333

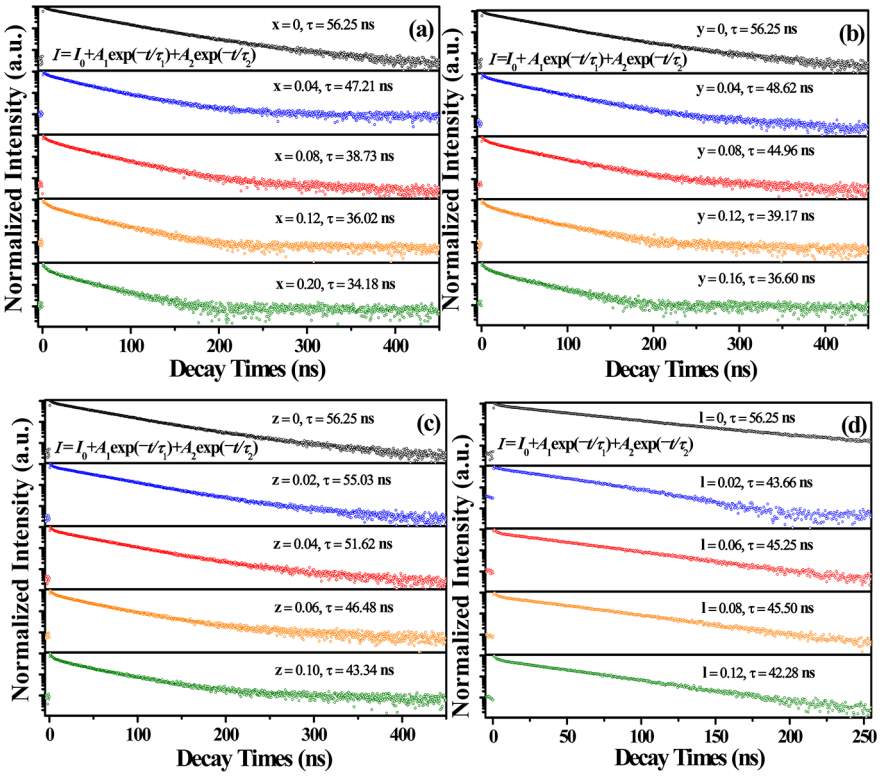

Figure 10. Decay curves of host emission in CNO:xEu^{3+} (a), CNO:yTb^{3+} (b), CNO:zDy^{3+} (c), and CNO:lSm^{3+} (d) with different activators concentrations.

Table 2. Decay Lifetimes of Host Emission in CNO:*x*Eu^{3+}/*y*Tb^{3+}/*z*Dy^{3+}/*l*Sm^{3+} Samples

CNO:xEu^{3+}/yTb^{3+}/zDy^{3+}/lSm^{3+} (λ_{ex} = 265 nm, λ_{em} = 460 nm)							
x	τ (ns)	y	τ (ns)	z	τ (ns)	l	τ (ns)
0	56.25	0	56.25	0	56.25	0	56.25
0.04	47.21	0.04	48.62	0.02	55.03	0.02	43.66
0.08	38.73	0.08	44.96	0.04	51.62	0.06	45.25
0.12	36.02	0.12	39.17	0.06	46.48	0.08	45.50
0.20	34.18	0.16	36.60	0.10	43.34	0.12	42.28

migration is hindered. Therefore, the R_c value can be roughly assessed by the calculation pointed out by Blasse:[63−65]

$$R_c = 2\left(\frac{3V}{4\pi X_c N}\right)^{1/3} \quad (5)$$

where V corresponds to the volume of the unit cell, N is the number of host cations in the unit cell, and X_c is the critical concentration of dopant ions. For the CNO host, N = 4, V = 446.79 Å^3, and X_c is 30%, 8%, and 6% for Eu^{3+}, Tb^{3+}, and Dy^{3+}, respectively; Accordingly, the R_c are estimated to be about 8.9, 13.86, and 15.26 Å.

In general, there are three mechanisms for nonradiate energy transfer including exchange interaction, radiation reabsorption and electric multipolar interactions. The R_c obtained above indicate the little possibility of exchange interaction since the exchange interaction is predominant only for about 5 Å.[66−68] The mechanism of radiation reabsorption is only efficacious when the fluorescence and absorption spectra are widely overlapping, which also does not intend to occur in these cases. As a result, we can infer that the electric multipolar interactions would be responsible for the energy transfer mechanisms from the host to activators. On account of Dexter's energy transfer formula of multipolar interactions and Reisfeld's approximation, the following relationship can be attained:[69,70]

$$\frac{\eta_{S_0}}{\eta_S} \propto C^{\alpha/3} \quad (6)$$

where η_{S_0} and η_S represent the luminescence quantum efficiencies of the host with the absence and presence of the Eu^{3+}/Tb^{3+}/Dy^{3+} ions, respectively. C is the concentration of the Eu^{3+}/Tb^{3+}/Dy^{3+} ions. The value for α = 6, 8, and 10 corresponds to dipole−dipole, dipole−quadrupole, and quadrupole−quadrupole interactions, respectively. However, the value of η_{S_0}/η_S is hard to obtain, and thus it can be approximately calculated instead by the I_{S_0}/I_S, where I_{S_0} and I_S stand for the luminescence intensity of the host without and with the Eu^{3+}/Tb^{3+}/Dy^{3} ions, respectively, the following relation can be obtained:[71−73]

$$\frac{I_{S_0}}{I_S} \propto C^{\alpha/3} \quad (7)$$

The relationship between I_{S_0}/I_S and $C^{\alpha/3}$ based on the above equation is illustrated in Figure 11, which can be respectively fitted using straight line. One can find that all the biggest R^2 values of the linear fittings occur when α = 6 in Figure 11a−c, corresponding to their respectively best linear behaviors. Therefore, the energy transfers from the host to Eu^{3+}/Tb^{3+}/Dy^{3+} ions take place through the dipole−dipole mechanisms.

Figure 12 shows a simple model expressing the energy transfer from $O^{2-} \rightarrow Nb^{5+}$ charge transfer band to Eu^{3+}, Tb^{3+}, Dy^{3+}, and Sm^{3+} ions and the characteristic emission energy levels of Eu^{3+}, Tb^{3+}, Dy^{3+}, and Sm^{3+} ions in CNO. In

dx.doi.org/10.1021/ic502493c | Inorg. Chem. 2015, 54, 323−333

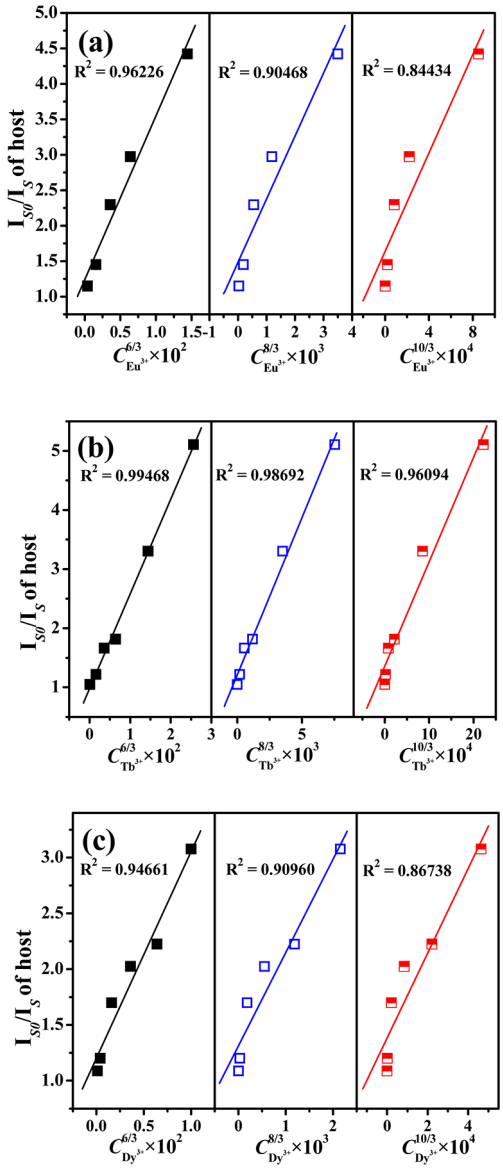

Figure 11. Dependence of I_{S_0}/I_S of host emission on $C^{6/3}$, $C^{8/3}$, and $C^{10/3}$ in CNO:Eu^{3+}/Tb^{3+}/Dy^{3+} (a–c), respectively.

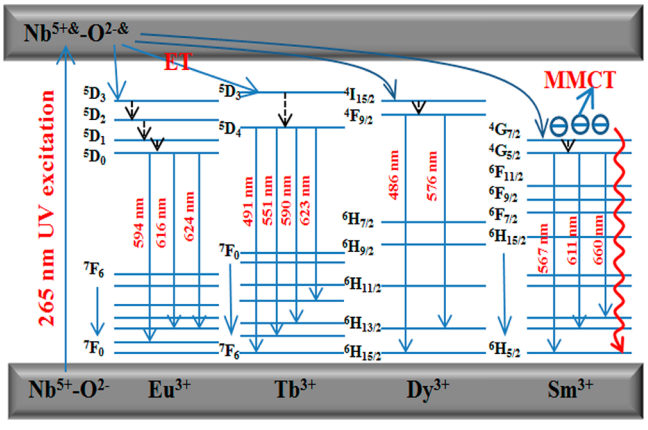

Figure 12. A simple model expressing the energy transfer from $O^{2-} \rightarrow Nb^{5+}$ charge transfer band to Eu^{3+}, Tb^{3+}, Dy^{3+}, and Sm^{3+} ions, the characteristic emission energy level of Eu^{3+}, Tb^{3+}, Dy^{3+}, and Sm^{3+} ions in CNO.

CNO:Eu^{3+}/Tb^{3+}/Dy^{3+} samples, upon 265 nm UV radiation, CNO absorb UV radiation and then the excitation energy is transferred from the NbO_6 group ($O^{2-} \rightarrow Nb^{5+}$ charge transfer band) to the respectively excited states of Eu^{3+}/Tb^{3+}/Dy^{3+} ions, which results in the increases of characteristic emission intensities of activators. When Sm^{3+} ions are doped into CNO, the situation changes a little. In CNO:Sm^{3+}, the NbO_6 group ($O^{2-} \rightarrow Nb^{5+}$ charge transfer band) absorbs UV radiation efficiently, and then the energy migrates to the $^4G_{7/2}$ energy level of Sm^{3+} ions. The excited electrons in this energy level can be readily transferred to the Nb^{4+}-Sm^{4+} CT state followed by the nonradiative relaxation (red curves) to the ground state $^5H_{5/2}$ of Sm^{3+}, leading to the loss of emission energy of Sm^{3+}. Only a small part of energy can be effectively contributed to Sm^{3+} emission. Therefore, the emission intensity of Sm^{3+} becomes weak and varies more obsoletely than that of Eu^{3+}/Tb^{3+}/Dy^{3+} ions.

In order to enrich the emission colors, the Eu^{3+} and Tb^{3+} codoped CNO phosphors were synthesized. Figure 13 shows

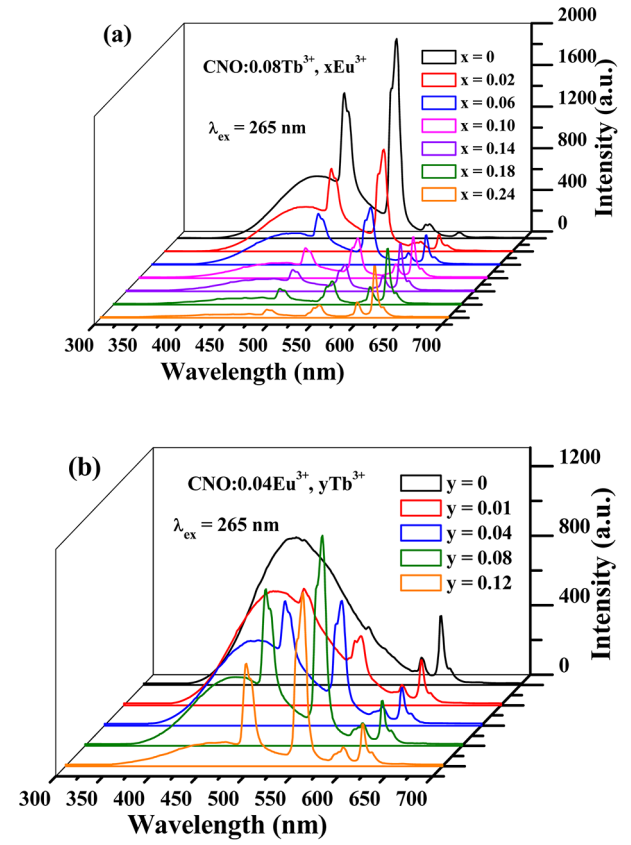

Figure 13. PL emission spectra of (a) CNO:0.08Tb^{3+}, $x$$Eu^{3+}$ and (b) CNO:0.04Eu^{3+}, $y$$Tb^{3+}$ samples as a function of Eu^{3+} and Tb^{3+} concentration, respectively.

the PL emission spectra for them upon 265 nm UV excitation. When Tb^{3+} is fixed at y = 0.08, the intensities of host and Tb^{3+} (at 551 nm) emissions both decrease while the Eu^{3+} emission intensity first increases and saturates at x = 0.18, as depicted in Figure 13a, which illustrates the energy transfers from the host and Tb^{3+} to Eu^{3+} ions. In CNO:0.04Eu^{3+}, yTb^{3+}, the emission intensity of Eu^{3+} when y = 0 is much stronger than that of y = 0.01, 0.04, 0.08, and 0.12 (the emission intensity of them are close). The emission intensity of host decreases monotonously, different from Tb^{3+} situation, which shows the original increase

dx.doi.org/10.1021/ic502493c | Inorg. Chem. 2015, 54, 323–333

until $y = 0.08$, and then the decrease occurs in Figure 13b. We can deduce that the energy transfer from the host to Tb^{3+} ions is more apt to that from the Tb^{3+} to Eu^{3+} ions from the phenomenon above.

Figure 14 presents the corresponding CIE (Commission Intemationale de I'Eclairage 1931 chromaticity) coordinates

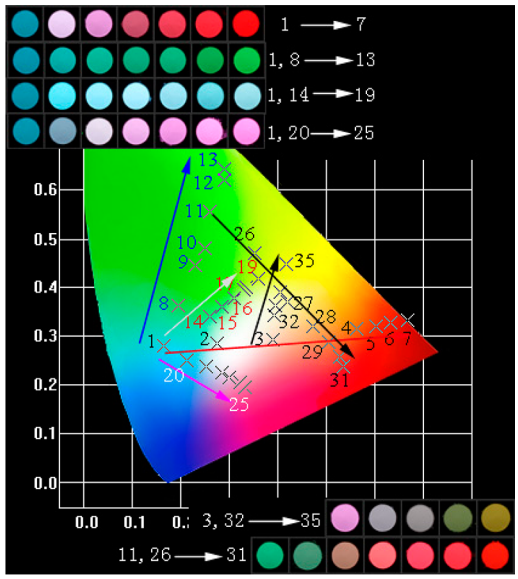

Figure 14. CIE chromaticity diagram for CNO:Eu^{3+} (point 1−7), Tb^{3+} (point 8−13), Dy^{3+} (point 14−19), CNO:Sm^{3+} (point 20−25), and CNO:Eu^{3+}, Tb^{3+} phosphors excited at 265 nm. Inset: digital photographs of them with increasing activators concentrations (along the direction of arrows) upon 254 nm UV lamp box excitation.

positions for the as-prepared CNO:Eu^{3+}/Tb^{3+}/Dy^{3+}/ Sm^{3+} and CNO:Eu^{3+}, Tb^{3+} samples under 265 nm UV excitation, as well as the different digital luminescence photographs upon 254 nm UV excitation. The corresponding obtained quantum efficiencies and chromaticity coordinates excited at 265 nm are listed in Table 3. It can be found that the CNO:Eu^{3+} samples can emit bright cyan to red light, and their chromaticity coordinate varies from $x = 0.165$, $y = 0.281$ (point 1) with the quantum efficiency of 40.5% to $x = 0.667$, $y = 0.333$ (point 7). The CNO:Tb^{3+} samples can emit cyan to bright green, whose chromaticity coordinate changes from $x = 0.165$, $y = 0.281$ (point 1) to $x = 0.289$, $y = 0.642$ (point 13). The CNO:Dy^{3+} samples show the luminescence color varies from cyan to light yellow, and the chromaticity coordinate is from $x = 0.165$, $y = 0.281$ (point 1) to $x = 0.361$, $y = 0.418$ (point 19). The CNO:Sm^{3+} samples show that the luminescence color varies from cyan to light pink with the corresponding chromaticity coordinates from $x = 0.165$, $y = 0.281$ (point 1) to $x = 0.333$, $y = 0.196$ (point 25). When the Eu^{3+} and Tb^{3+} are codoped into the host, the tunable color can be seen from green to red, which coincides with the chromaticity coordinate of $x = 0.259$, $y = 0.556$ (point 11) to $x = 0.536$, $y = 0.238$ (point 31) and $x = 0.389$, $y = 0.293$ (point 3) to $x = 0.417$, $y = 0.448$ (point 35) along the black arrow in Figure 14. In all as-prepared samples, the maximum quantum efficiency is 71.2% for CNO:0.01/0.02Dy^{3+}.

4. CONCLUSIONS

In summary, a series of Ln^{3+} (Ln^{3+} = Eu^{3+}/Tb^{3+}/Dy^{3+}/Sm^{3+}) ions doped $CaNb_2O_6$ (CNO) phosphors have been prepared

Table 3. Variation of Quantum Yields (QYs) Corresponding Variations of CIE Chromaticity Coordinate for CNO:Eu^{3+}/Tb^{3+}/Dy^{3+}/Sm^{3+} Phosphors Excited under 265 nm UV radiation

no. of points	CNO:xEu^{3+}/yTb^{3+}/zDy^{3+}/Sm^{3+}	QYs/%	CIE (x, y)
1	$x = 0$	40.5	(0.165, 0.281)
2	$x = 0.02$	34.6	(0.274, 0.284)
3	$x = 0.04$	30.1	(0.389, 0.293)
4	$x = 0.08$	27.3	(0.563, 0.316)
5	$x = 0.12$	25.4	(0.608, 0.320)
6	$x = 0.20$	31.1	(0.637, 0.325)
7	$x = 0.03$	35.6	(0.667, 0.333)
8	$y = 0.01$	43.9	(0.194, 0.363)
9	$y = 0.04$	41.9	(0.229, 0.446)
10	$y = 0.06$	39.9	(0.249, 0.480)
11	$y = 0.08$	26.4	(0.259, 0.556)
12	$y = 0.10$	22.4	(0.289, 0.619)
13	y = 0.12	17.4	(0.291, 0.642)
14	$z = 0.01$	71.2	(0261, 0.340)
15	$z = 0.02$	71.2	(0.284, 0.359)
16	$z = 0.04$	60.9	(0.309, 0.478)
17	$z = 0.06$	47.8	(0.331, 0.394)
18	$z = 0.08$	53.9	(0.336, 0.399)
19	$z = 0.10$	36.7	(0.361, 0.418)
20	$l = 0.01$	40.0	(0.232, 0.250)
21	$l = 0.02$	38.4	(0.252, 0.238)
22	$l = 0.04$	35.5	(0.284, 0.225)
23	$l = 0.06$	30.6	(0.310, 0.215)
24	$l = 0.08$	32.2	(0.322, 0.205)
25	$l = 0.12$	30.2	(0.333, 0.196)
no. of points	CNO:0.08Tb^{3+}, xEu^{3+}	QYs/%	CIE (x, y)
11	$x = 0$	21.2	(0.259, 0.556)
26	$x = 0.02$	20.8	(0.353, 0.471)
27	$x = 0.06$	19.1	(0.419, 0.371)
28	$x = 0.10$	22.7	(0.473, 0.320)
29	$x = 0.14$	23.6	(0.504, 0.288)
30	$x = 0.18$	24.9	(0.527, 0.258)
31	$x = 0.24$	22.3	(0.536, 0.238)
no. of points	CNO:0.04Eu^{3+}, yTb^{3+}	QYs/%	CIE (x, y)
3	$y = 0$	30.1	(0.389, 0.293)
32	$y = 0.01$	25.7	(0.392, 0.343)
33	$y = 0.04$	23.3	(0.396, 0.364)
34	$y = 0.08$	28.3	(0.405, 0.391)
35	$y = 0.12$	22.2	(0.417, 0.448)

via the conventional high-temperature solid-state reaction route. The Rietveld refinements of powder XRD profiles of representative samples demonstrate the purity phase of as-synthesized samples. Upon 265 nm UV excitation, the CNO host can emit a broad band from 355 to 605 nm centered at 460 nm owing to the charge transfer band (CTB) from O ligands to central Nb atoms in the NbO_6 octahedral groups. When Eu^{3+}/Tb^{3+}/Dy^{3+}/Sm^{3+} were doped into the hosts, the excitation spectra of characteristic 4f−4f transitions emissions for Eu^{3+}/Tb^{3+}/Dy^{3+}/Sm^{3+} are similar to the host one, which illustrates the existence of energy transfer from host to activators. The samples present various emission colors attributed to the energy transfer from host to activators with increasing activators concentrations upon 265 nm UV excitation. However, the characteristic emission intensity of Sm^{3+} for CNO:Sm^{3+} is much weaker than that of CNO:Eu^{3+}/Tb^{3+}/Dy^{3+}, which may be ascribed to the metal−metal charge

dx.doi.org/10.1021/ic502493c | Inorg. Chem. 2015, 54, 323−333

transfer transition (MMCT) of $Nb^{5+}+Sm^{3+} \rightarrow Nb^{4+}+Sm^{4+}$. The monotonous decreases of decay lifetimes of host emission in CNO:Eu^{3+}/Tb^{3+}/Dy^{3+} certify the existence of energy transfer from host to activators in CNO:Eu^{3+}/Tb^{3+}/Dy^{3+} with increasing activators concentrations, whereas the decay lifetime of host emission in CNO:Sm^{3+} does not decrease monotonously, which also may originate from the MMCT. The energy transfer mechanisms from host to activators have been demonstrated to be dipole−dipole interactions in CNO:Eu^{3+}/Tb^{3+}/Dy^{3+}. The best quantum efficiency is 71.2% for CNO:0.01/0.02Dy^{3+}. The PL properties have shown that these materials might have potential for UV-pumped WLEDs field.

AUTHOR INFORMATION

Corresponding Authors

*(J.L.) E-mail: jlin@ciac.ac.cn.

*(H.L.) E-mail: hzlian@ciac.ac.cn.

Notes

The authors declare no competing financial interest.

ACKNOWLEDGMENTS

This project is financially supported by the National Natural Science Foundation of China (51332008, 91433110, 51172227, and 51472234), National Basic Research Program of China (2014CB643803), and Joint Funds of the National Natural Science Foundation of China (U13012042).

REFERENCES

(1) Jüstel, T.; Nikol, H.; Ronda, C. *Angew. Chem., Int. Ed.* **1998**, *37*, 3084−3103.

(2) Wang, S.-S.; Chen, W.-T.; Li, Y.; Wang, J.; Sheu, H.-S.; Liu, R.-S. *J. Am. Chem. Soc.* **2013**, *135*, 12504−12507.

(3) Tsang, M. K.; Chan, C. F.; Wong, K. L.; Hao, J. *J. Lumin.* **2015**, *157*, 172−178.

(4) Schafer, H.; Ptacek, P.; Eickmeier, H.; Haase, M. *Adv. Funct. Mater.* **2009**, *19*, 3091−3097.

(5) Kim, D.; Jang, J.; Ahn, S.; Kim, S.-H.; Park, J.-C. *J. Mater. Chem. C* **2014**, *2*, 2799−2805.

(6) Zhang, Y.; Hao, J. *J. Mater. Chem. C* **2013**, *1*, 5607−5618.

(7) Wang, Y.; Brik, M. G.; Dorenbos, P.; Huang, Y.; Tao, Y.; Liang, H. *J. Phys. Chem. C* **2014**, *118*, 7002−7009.

(8) Holloway, P. H.; Trottier, T.; Abrams, A. B.; Kondoleon, C.; Jones, S. L.; Sebastian, J. S.; Thomes, W. J.; Swart, H. *J. Vac. Sci. Technol. B* **1999**, *17*, 758−764.

(9) Liu, Y. H.; Zhuang, W. D.; Hu, Y. S.; Gao, W. G.; Hao, J. H. *J. Alloys Compd.* **2010**, *504*, 488−492.

(10) McKittrick, J.; Shea, L. E.; Bacalski, C. F.; Bosze, E. J. *Displays* **1999**, *19*, 169−172.

(11) Tsang, M.-K.; Bai, G.; Hao, J. H. *Chem. Soc. Rev.* **2015**, DOI: 10.1039/C4CS00171K.

(12) Lee, G.; Han, J. Y.; Im, W. B.; Cheong, S. H.; Jeon, D. Y. *Inorg. Chem.* **2012**, *51*, 10688−10694.

(13) Yu, H.; Deng, D.; Zhou, D.; Yuan, W.; Zhao, Q.; Hua, Y.; Zhao, S.; Huang, L.; Xu, S. *J. Mater. Chem. C* **2013**, *1*, 5577−5582.

(14) Zhong, J.; Zhao, W.; Lan, L.; Wang, J.; Chen, J.; Wang, N. *J. Alloys Compd.* **2014**, *592*, 213−219.

(15) Xia, Z.; Liu, R.-S.; Huang, K.-W.; Drozd, V. *J. Mater. Chem.* **2012**, *22*, 15183−15189.

(16) Xia, Z.; Liu, R.-S. *J. Phys. Chem. C* **2012**, *116*, 15604−15609.

(17) Guo, N.; Huang, Y.; Yang, M.; Song, Y.; Zheng, Y.; You, H. *Phys. Chem. Chem. Phys.* **2011**, *13*, 15077−15082.

(18) Zhou, X.; Yang, X.; Xiao, T.; Zhou, K.; Chen, T.; Yan, H.; Wang, Z. *J. Rare Earths* **2013**, *31*, 655−659.

(19) Natarajan, V.; Dhobale, A. R.; Lu, C.-H. *J. Lumin.* **2009**, *129*, 290−293.

(20) Li, K.; Shang, M.; Geng, D.; Lian, H.; Zhang, Y.; Fan, J.; Lin, J. *Inorg. Chem.* **2014**, *53*, 6743−6751.

(21) Wang, Z.; Teng, X.; Li, P. *J. Alloys Compd.* **2014**, *592*, 549−554.

(22) Liu, H.; Liao, L.; Xia, Z. *RSC Adv.* **2014**, *4*, 7288−7295.

(23) Yang, Z.; Hou, C.; Duan, G.; Yang, Fu.; Liu, P.; Wang, C.; Liu, L.; Dong, G. *J. Alloys Compd.* **2014**, *604*, 346−351.

(24) Cao, C.; Yang, H. K.; Moon, B. K.; Choi, B. C.; Jeong, J. H. *J. Electrochem. Soc.* **2010**, *158*, J6−J9.

(25) AsiriNaidu, S.; Boudin, S.; Varadaraju, U. V.; Raveau, B. *J. Solid State Chem.* **2011**, *184*, 2566−2570.

(26) Chen, Y.; Wang, J.; Liu, C.; Kuang, X.; Su, Q. *Appl. Phys. Lett.* **2011**, *98*, 081917.

(27) Francis, L. T.; Rao, P.; Thomas, M.; Mahesh, S. K.; Reshmi, V. R.; Thampi, V. D. S. *Mater. Lett.* **2012**, *81*, 142−144.

(28) Blasse, G.; Bril, A. *J. Lumin.* **1970**, *3*, 109−131.

(29) Lv, Y.; Tang, X.; Yan, L.; Li, K.; Liu, X.; Shang, M.; Li, C.; Lin, J. *J. Phys. Chem. C* **2013**, *117*, 21972−21980.

(30) Massabni, A. M. G.; Montandon, G. J. M.; Couto dos Santos, M. A. *Mater. Res.* **1998**, *1(a)*, 1−4.

(31) Teixeira, N. G.; Moreira, R. L. *Cryst. Growth Des.* **2011**, *11*, 3472−3478.

(32) Zhang, Y.; Liu, C.; Pang, G.; Jiao, S.; Zhu, S.; Wang, D.; Liang, D.; Feng, S. *Eur. J. Inorg. Chem.* **2010**, *8*, 1275−1282.

(33) Li, J. H.; Liu, X. H.; Wu, J. B.; Zhang, X. Y.; Li, L.; Zhang, Y. C.; Fu, X. H. *Laser Phys. Lett.* **2012**, *9*, 199−203.

(34) Singh, K. N.; Bajpai, P. K. *J. Inter. Acad. Phys. Sci.* **2010**, *14*, 129−138.

(35) Zhou, R.; Wei, X.; Duan, C.; Chen, Y.; Yin, M. *ECS J. Solid State Sci. Technol.* **2012**, *1*, R147−R152.

(36) Boutinaud, P.; Cavalli, E.; Bettinelli, M. *J. Phys.: Condens. Matter* **2007**, *19*, 386230.

(37) Huang, J.; Zhou, L.; He, X.; Gong, F. *Chin. J. Chem.* **2011**, *29*, 441−445.

(38) Wang, Y.; Zhang, L.; Cao, R.; Miao, Q.; Qiu, J. *Appl. Phys. A: Mater. Sci. Process.* **2014**, *115*, 1365−1370.

(39) Cummings, J. P.; Simonsen, S. H. *Am. Mineral.* **1970**, *55*, 90−91.

(40) Mathai, K. C.; Vidya, S.; John, A.; Solomon, S.; Thomas, J. K. *Adv. Condens. Matter Phys.* http://dx.doi.org/10.1155/2014/735878.

(41) Zeng, W.; Wang, Y.; Han, S.; Chen, W.; Li, G.; Wang, Y.; Wen, Y. *J. Mater. Chem. C* **2013**, *1*, 3004−3011.

(42) Xia, Z.; Zhang, Y.; Molokeev, M. S.; Atuchin, V. V. *J. Phys. Chem. C* **2013**, *117*, 20847−20854.

(43) Xia, Z.; Zhou, J.; Mao, Z. *J. Mater. Chem. C* **2013**, *1*, 5917−5924.

(44) Ma, Q.; Lu, M.; Yang, P.; Zhang, A.; Cao, Y. *Mater. Res. Bull.* **2013**, *48*, 3677−3686.

(45) Belsky, A.; Krupa, J. *Displays* **1999**, *19*, 185−196.

(46) Hsu, C.; Powell, R. C. *J. Lumin.* **1975**, *10*, 273−293.

(47) Blasse, G.; Grabmarier, B. C. *Luminescent Materials*; Springer-Verlag: Berlin, Germany, 1994.

(48) Li, G.; Zhang, Y.; Geng, D.; Shang, M.; Peng, C.; Cheng, Z.; Lin, J. *ACS Appl. Mater. Interfaces* **2012**, *4*, 296−305.

(49) Jia, Y.; Qiao, H.; Zheng, Y.; Guo, N.; You, H. *Phys. Chem. Chem. Phys.* **2012**, *14*, 3537−3542.

(50) Luo, W.; Li, R.; Chen, X. *J. Phys. Chem. C* **2009**, *113*, 8772−8777.

(51) Han, B.; Liang, H.; Huang, Y.; Tao, Y.; Su, Q. *Appl. Phys. B: Laser Opt.* **2011**, *104*, 241−246.

(52) Niu, N.; Yang, P.; Wang, W.; He, F.; Gai, S.; Wang, D.; Lin, J. *Mater. Res. Bull.* **2011**, *46*, 333−339.

(53) Reddy. S. Das, A. A.; Goel, A.; Sen, R.; Siegel, R.; Mafra, L.; Vijaya Prakash, G.; Ferreira, J. M. F. *AIP Adv.* **2013**, *3*, 022126.

(54) Huang, P.; Chen, D.; Wang, Y. *J. Alloys Compd.* **2011**, *509*, 3375−3381.

(55) Lee, K. H.; Choi, S.; Jung, H.-K.; Im, W. B. *Acta Mater.* **2012**, *60*, 5783−5790.

(56) Guo, N.; Song, Y.; You, H.; Jia, G.; Yang, M.; Liu, K.; Zheng, Y.; Huang, Y.; Zhang, H. *Eur. J. Inorg. Chem.* **2010**, *29*, 4636−4642.

(57) Liang, Z.; Mo, F.; Zhang, X.; Zhou, L.; Chen, P.; Xu, C. *Ceram. Int.* **2014**, *40*, 7501−7508.

(58) Yang, W. J.; Chen, T. M. *Appl. Phys. Lett.* **2006**, *88*, 101903.
(59) Hu, S.; Tang, W. *J. Lumin.* **2014**, *145*, 100−104.
(60) Jiang, T.; Yu, X.; Xu, X.; Yu, H.; Zhou, D.; Qiu, J. *Mater. Res. Bull.* **2014**, *51*, 80−84.
(61) Murakami, S.; Herren, M.; Rau, D.; Morita, M. *Inorg. Chim. Acta* **2000**, *300*−*302*, 1014−1021.
(62) Huang, C. H.; Chen, T. M.; Liu, W. R.; Chiu, Y. C.; Yeh, Y. T.; Jang, S. M. *ACS Appl. Mater. Interfaces* **2010**, *2*, 259−264.
(63) Wen, D.; Shi, J. *Dalton Trans.* **2013**, *42*, 16621−16629.
(64) Blasse, G. *J. Solid, State. Chem.* **1986**, *62*, 207−211.
(65) Zhang, X.; Zhang, J.; Gong, M. *Opt. Mater.* **2011**, *33*, 909−913.
(66) Dexter, D. L. *J. Chem. Phys.* **1953**, *21*, 836−850.
(67) Liu, W. R.; Huang, C. H.; Wu, C. P.; Chiu, Y. C.; Yeh, Y. T.; Chen, T. M. *J. Mater. Chem.* **2011**, *21*, 6869−6874.
(68) Wen, D.; Dong, Z.; Shi, J.; Gong, M.; Wu, M. *ECS J. Solid State Sci. Technol.* **2013**, *2*, R178−R185.
(69) Dexter, D. L.; Schulman, J. H. *J. Chem. Phys.* **1954**, *22*, 1063−1070.
(70) Blasse, G. *Philips Res. Rep.* **1969**, *24*, 131−144.
(71) Huang, C.-H.; Chan, T.-S.; Liu, W.-R.; Wang, D.-Y.; Chiu, Y.-C.; Yeh, Y.-T.; Chen, T.-M. *J. Mater. Chem.* **2012**, *22*, 20210−20216.
(72) Li, Y.; Li, H.; Liu, B.; Zhang, J.; Zhao, Z.; Yang, Z.; Wen, Y.; Wang, Y. *J. Phys. Chem. Solids* **2013**, *74*, 175−180.
(73) Paulose, P. I.; Jose, G.; Thomas, V.; Unnikrishnan, N. V.; Warrier, M. K. R. *J. Phys. Chem. Solids* **2003**, *64*, 841−846.